A new approach for torque ripple reduction in a faulty surface permanent magnet synchronous motor by inverse current injection

Elmehdi Bahri, Rémus Pusca, Driss Belkhayat, Raphael Romary

A new approach for torque ripple reduction in a faulty Surface Permanent Magnet Synchronous Motor by inverse current injection

Elmehdi Bahri[a,b], Rémus Pusca[a], Raphael Romary[a*], Driss Belkhayat[b]
[a] Univ. Artois, EA 4025, LSEE, Béthune,F-62400 France
[b] LSET, Cadi Ayyad University, BP 549, Av Abdelkarim Elkhattabi, Gueliz, Marrakech, Morocco
[*]raphael.romary@univ-artois.fr.

Abstract -- The aim of this paper is to present a new method to generate stator currents supplying a Surface Permanent Magnets Synchronous Motor (SPMSM) presenting an asymmetry of the stator windings. This asymmetry may be due to a lack of turns in one of the stator windings or to an inter-turns short circuit. An analytical model of the SPMSM is developed to calculate the current which allows minimizing the torque ripple generated by the asymmetry. This model is based on the combination of the space harmonics of the flux densities of stator and rotor for the generation of the torque. Our study leads to define a stator inverse current system able to compensate the harmonic torque component at the double of the supply frequency. In the experimental tests, several cases of supply were applied and the results confirmed those obtained by the analytical study essentially concerning the amplitude of the inverse current.

Keywords: Permanent magnet synchronous motor, torque ripple, vibrations, winding asymmetry.

List of symbols

α^s (rad): Angular abscissa of the point M, related to the stator reference axis.
α^r (rad): Angular abscissa of the point M, related to the rotor reference axis.
β_j^s (rad): Angular position of the stator slot j.
Γ_h : Coefficient linked to the linear evolution of the mmf along the slot width.
δ (m): Half slot width $\delta = (1 - r_d^s)\pi / N_t^s$.
ε_{0j}^s(A): Magnetomotive force created by conductors contained in the slot j.
ε_0^s(A): Total magnetomotive force generated by all slots.
θ (rad): Rotor position related to the stator reference axis.
μ_0 (H/m): Vaccum permeability.
φ_j (rad): Current phase angle in the slot j.
φ_n^r (rad): Phase of the rotor flux density space harmonic relating to the fundamental.
φ_h^s (rad): Phase of the stator flux density space harmonic relating to the fundamental.
ω (rad/s): supply angular frequency.
b^s (T): Stator flux density.
b^r (T): Rotor flux density.
e (m): Minimum air gap thickness.
h : mmf space harmonic rank.
i_j^s (A): Current flowing in the conductors of slot j.
k_s : Permeance rank.
K : Ratio of faulty turn in one slot.
l_e^s (m): Stator slot width.
l_d^s (m): Stator tooth width.
mmf : Magnetomotive force.
N_t^s : Total stator slot number.
n_e : Number of conductors in stator slot.
n_{jdef}^e : Conductors number in faulty slot j.
p : Pole pair number.
P (H): Air gap permeance.

p^s (m): Stator fictive slot depth.

R_s (m): Stator inner radius

r_d^s : Stator toothing ratio $r_d^s = \frac{l_d^s}{l_d^s + l_e^s}$.

V (m^3): Total volume of the air gap.

Wmag (J): Magnetic co-energy

1. Introduction

The Permanent Magnet Synchronous Motor (SPMSM) is widely used in various fields such as industry, electric vehicles, aircraft, etc. This is mainly due to its high performance, high torque density, robust brushless construction, etc. [1, 2]. The tangential vibrations generated by the SPMSM and the iron losses in the rotor are factors that reduce its performance and efficiency and consequently its use [3-5].

The occurrence of a fault such as a winding unbalance, a rotor demagnetization, an inter-turns short-circuit or an eccentricity results in the increase of the tangential vibrations and also the losses [6, 8, 9, 10]. Significant lack of reliability of the global system may occur if the power supply control does not take into account the fault [11, 12]. This is especially true for applications such as electric vehicles and aerospace systems [13].

The reduction of tangential vibrations in a healthy synchronous machine has been studied in several researches and numerous strategies have been proposed in this field [14]. The best known strategy is to control the stator currents to compensate the torque ripple as indicated in [15-17]. These currents are determined by several methods. Some of these methods use the Fourier series decomposition of the electromotive force to obtain a limited number of current harmonics. Others use the finite element method to determine harmonic currents [18-20]. Other control strategies are based on the analytical modeling of the machine to obtain the harmonic currents by performing an optimization test [21].

Concerning the faulty SPMSM, numerous studies have been carried out for its modeling and control especially for multiphase motors. Some methods use a vector approach to calculate the optimal current reference [22]. In this work the calculation of the currents is based on maintaining a smooth torque and minimal joule losses. The electromotive force vectors allow the determination of the current reference in real time. Other methods for three phase motor [8] are based on the dynamic modeling of the faulty machine using the mathematical equations of the flux. The separation of voltages and currents in direct and inverse components are also taken into account. The purpose of the control strategy is to cancel the inverse component using two current controllers. There is also a control method for a three phase motor with special stator winding architecture where all the phases are electrically isolated and able to support twice the rated current, so that the motor can provide the nominal torque even if only 2 phases are supplied [23]. In [24], it is proposed to change the supply in faulty conditions in order to mitigate the short circuit current. But none of these works studies the electrical motor with the objective to find the real origin of the fault and to give a method to estimate its magnitude, that can be used in the control system.

The aim of this work is to define a control strategy to compensate the effect of the stator winding asymmetry and therefore to minimize the torque ripple. The analytical method is based on the cancellation of the negative sequence of the air gap flux density. As reported in [8], the principle of many researches is to cancel the negative sequence current, but this method is not sufficient for the torque ripple. It will be shown that the faulty winding generates negative sequence of air gap flux density even when the motor is supplied by a positive sequence current. In this paper, the asymmetry will be generated, at first, by a lack of turns of approximately 11% of a stator phase winding.

This paper is organized as follows: in the first part, the used analytical approach is presented. Then, the effects giving rise to torque harmonics, especially those generated by the space harmonics are identified. The relationship between these harmonics and the torque is expressed in a condensed equation depending on the parameters of the SPMSM. In the second part, a comparative study of the torque harmonics generated in the two cases (healthy SPMSM and faulty SPMSM) is performed. The simulation results concerning the control law to minimize the torque ripple are presented in the next part. Finally, experimental results are provided to validate the effectiveness of the proposed supply strategy in case of faulty winding by a lack of turns.

2. SPMSM analytical modeling

According to previous works [25], stator and rotor flux densities include fundamental components which generate the average torque and space harmonics responsible for the iron losses and the torque ripple [26-28]. In our analytical model a simplified method is presented to show the link between the torque harmonics and the flux density space harmonics relative to the stator and the rotor. Fig. 1.a shows the geometry of the studied machine. Here the stator yoke of the SPMSM contains 36 slots. The rotor yoke is smooth and has two pole pairs.

2.1. Stator flux density

In this study, the analytical modeling is based on the calculation of the torque using stator and rotor flux densities. The stator flux density is given by multiplying the stator magnetomotive force with the air gap permeance [29].

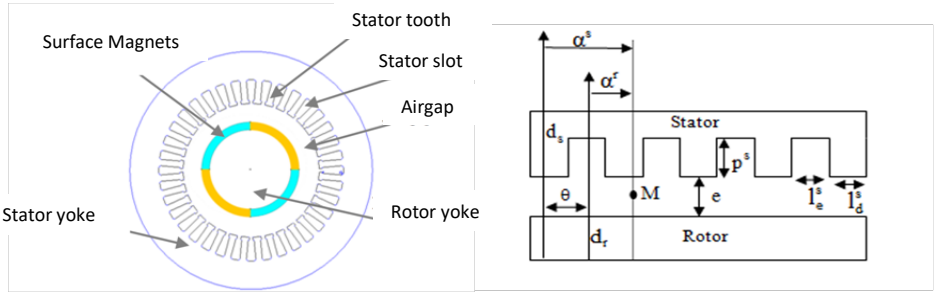

Fig.1. Model of the considered machine
(a) Geometry with $N_t^s = 36$ and p=2, (b) simplified model adopted for stator slots.

The permeance is proportional to the inverse of the air gap thickness and depends only on the shape of stator slots (Fig. 1.a). Adopting a simplified fictitious model for the slots (Fig. 1.b) resulting from the hypothesis that the rotor is smooth, the tooth has a rectangular shape and the slot depth is equal to one fifth of its width, the air gap permeance can be expressed as follows :

$$P = P_0 + \sum_{k_s=1}^{+\infty} P_{k_s} \cos(k_s N_t^s \alpha^s) \tag{1}$$

with $$P_0 = \mu_0 \frac{1}{(e + p^s)} \left(1 + \frac{p^s r_d^s}{e}\right)$$

and $$P_{k_s} = 2\mu_0 \frac{p^s}{e(e+p^s)} \frac{\sin(k_s r_d^s \pi)}{k_s \pi}$$

The point M in the air gap can be identified by its angular abscissa α^s related to the stator referential d_s and also its angular abscissa α^r related to the rotor referential d_r. So the angle θ related to the rotor position is given by $\theta = \alpha^s - \alpha^r$ (Fig.1.b).

The magnetomotive force generated by n_e conductors located in the slot j and flowed through by a current $i_j^s = \sqrt{2}\, I_j^s \sin(\omega t + \varphi_j)$ is expressed by:

$$\varepsilon_j^s = \frac{n_e i_j^s}{(\pi - \delta)} \sum_{h=1}^{+\infty} \Gamma_h \frac{\sin\left(h(\alpha^s - \beta_j^s)\right)}{h} \tag{2}$$

with

$$\Gamma_h = \frac{\sin[h(1 - r_d^s)\pi / N_t^s]}{h(1 - r_d^s)\pi / N_t^s}$$

The main advantage of using the slot mmf ε_j^s is that the machine can be easily modeled in faulty case. The total mmf generated by all the slots can be written as:

$$\varepsilon^s = \sum_{j=1}^{N_t^s} \varepsilon_j^s \tag{3}$$

A coil of a 4 pole stator winding is shown in Fig.2. It is composed of two coils; one has a side inserted into slot 1 and the other side inserted into slot 2. The mmf generated by the strands inserted in slots 1 and 2, and the resulting mmf is shown in Fig. 3.a. A zoom of the mmf created by slot 1 is shown in Fig.3.b. A linear evolution of mmf over the slot opening can be observed. Thus the stator flux density is given by:

$$b^s(\alpha^s) = P\varepsilon^s \tag{4}$$

Substituting P by its expression (1), the stator flux density is expressed as:

$$b^s(\alpha^s) = b_0^s(\alpha^s) + b_{k_s}^s(\alpha^s) \tag{5}$$

with $b_0^s(\alpha^s) = P_0 \varepsilon^s$ and $b_{k_s}^s(\alpha^s) = \varepsilon^s \sum_{k_s=1}^{+\infty} P_{k_s} \cos(k_s N_t^s \alpha^s)$

Therefore, it leads to:

$$b_0^s(\alpha^s) = \sum_{j=1}^{N_t^s} \sum_{\substack{h=-\infty \\ (h\neq 0)}}^{+\infty} \frac{P_0 n_e I_j^s}{\sqrt{2}(\pi - \delta)} \Gamma_h \frac{\cos[\omega t - h\alpha^s + (h\beta_j^s + \varphi_j)]}{h}$$

and

$$b_{k_s}^s(\alpha^s) = \sum_{j=1}^{N_t^s} \sum_{\substack{h=-\infty \\ (h\neq 0)}}^{+\infty} \frac{n_e I_j^s}{2\sqrt{2}h(\pi - \delta)} \Gamma_h \sum_{k_s}^{+\infty} P_{k_s} [\cos(\omega t - h\alpha^s + (h\beta_j^s + \varphi_j) - k_s N_t^s \alpha^s) + \cos(\omega t - h\alpha^s + (h\beta_j^s + \varphi_j) + k_s N_t^s \alpha^s)]$$

The stator flux density can be expressed with the following concise equation:

$$b^s(\alpha^s) = \sum_{\substack{h=-\infty \\ (h\neq 0)}}^{+\infty} B_h^s \cos(\omega t - h\alpha^s + \varphi_h^s) \tag{6}$$

where B^s_h the magnitude and φ_h^s the phase of the stator flux density space harmonic, are calculated using numerical implementation. Each harmonic of rank h rotates at the angular speed of ω/h.

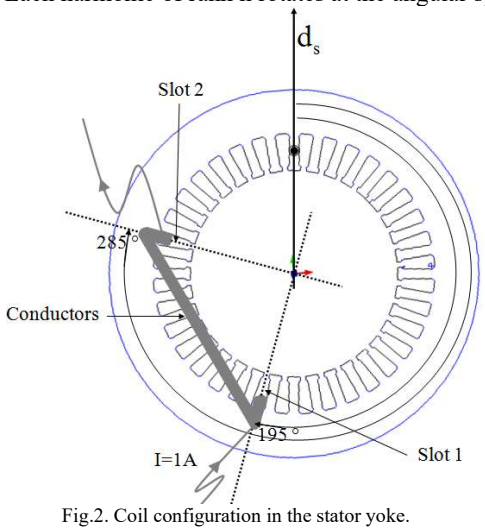

Fig.2. Coil configuration in the stator yoke.

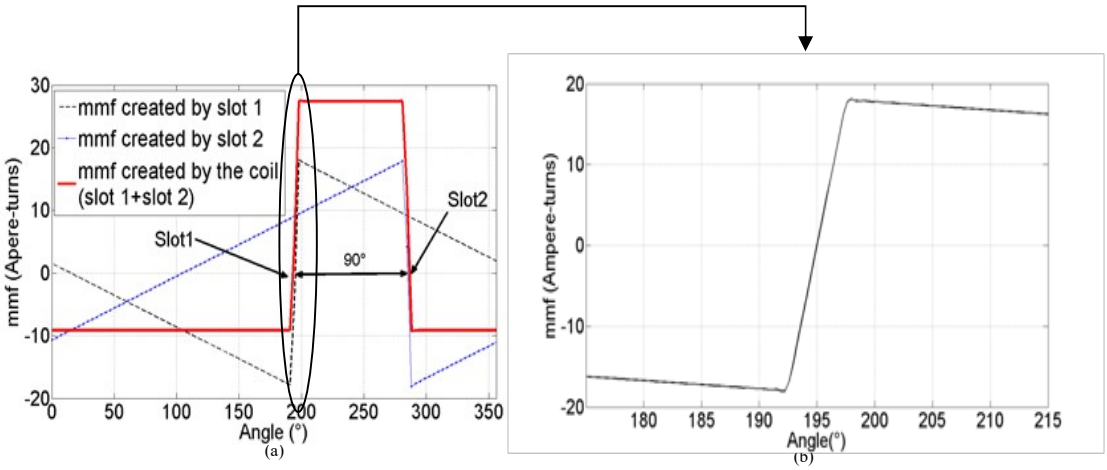

Fig.3. Evolution of the magnetomotive force created by:
(a) the conductors into two slots and the resulting component. (b) the conductors housed in slot 1.

2.2. Rotor flux density

The rotor flux density of a synchronous machine can be expressed as: [30]

$$b^r(\alpha^s) = \sum_{n=1,3,5}^{+\infty} B_n^r \cos(np\alpha^s - np\theta + \varphi_n^r) \tag{7}$$

where B_n^r is the magnitude of rotor flux density space harmonic.

2.3. Torque

The torque generated by a SPMSM [31] is of three types: the cogging torque, the reluctant torque, and the main electromagnetic torque produced by the interaction between the stator and rotor flux densities. The latter is the most important one. In this paper, only the electromagnetic torque is considered. It is given, using the magnetic co-energy Wmag, as:

$$C = \frac{\partial}{\partial\theta}\left(W_{mag}\right)$$

It comes:

$$C = \frac{\partial}{\partial\theta}\left(\frac{V}{\mu_0}\int_0^{2\pi} b^s b^r d\alpha^s\right) \tag{8}$$

where V is the total volume of the air gap. Considering Equ. (6) and (7), the electromagnetic torque C becomes:

$$C = \frac{\partial}{\partial\theta}\left(\frac{V}{\mu_0}\int_0^{2\pi}\frac{1}{2}\sum_{n,h} B_n^r B_h^s \begin{bmatrix}\cos\left(\omega t - (h - np)\alpha^s - np\,\theta + \varphi_h^s + \varphi_n^r\right) \\ + \cos\left(\omega t - (h + np)\alpha^s + np\,\theta + \varphi_h^s - \varphi_n^r\right)\end{bmatrix} d\alpha^s\right)$$

For this expression the integral is zero excepted for h=np and h=-np. Consequently, the torque can be divided into two terms according to the two conditions: -h+np=0 and -h-np=0. So the electromagnetic torque can be written as:

$$C = C^{-h+np=0} + C^{h+np=0}$$

with

$$C^{-h+np=0} = \frac{\partial}{\partial\theta}\left(\frac{V\pi}{\mu_0}\sum_{n=1,3,5}^{+\infty}\sum_{\substack{h=-\infty \\ (h\neq 0)}}^{h=+\infty} B_n^r B_h^s \cos\left(\omega t - np\theta + \varphi_h^s + \varphi_n^r\right)\right)$$

$$C^{h+np=0} = \frac{\partial}{\partial\theta}\left(\frac{V\pi}{\mu_0}\sum_{n=1,3,5}^{+\infty}\sum_{\substack{h=-\infty \\ (h\neq 0)}}^{h=+\infty} B_n^r B_h^s \cos\left(\omega t + np\theta + \varphi_h^s - \varphi_n^r\right)\right)$$

At steady state operation, the rotor position θ is: $\theta = \omega t/p + \theta_0$ where θ_0 is the initial rotor position and the above torque equations become:

$$C^{-h+np=0} = \frac{-Vp\pi}{\mu_0}\sum_{n=1,3,5}^{+\infty}\sum_{\substack{h=-\infty \\ (h\neq 0)}}^{h=+\infty} nB_n^r B_h^s \sin\left((1-n)\omega t - np\theta_0 + \varphi_h^s + \varphi_n^r\right) \quad (9)$$

and

$$C^{h+np=0} = \frac{-V\pi\pi}{\mu_0}\sum_{n=1,3,5}^{+\infty}\sum_{\substack{h=-\infty \\ (h\neq 0)}}^{h=+\infty} nB_n^r B_h^s \sin\left((1+n)\omega t + np\theta_0 + \varphi_h^s - \varphi_n^r\right) \quad (10)$$

3. Simulation of the stator flux density and torque ripple

To evaluate the impact of spatial harmonics on torque ripple, the theoretical equations of the stator and rotor flux densities for SPMSM, presented in Fig. 1, and also its torque are numerically implemented. Here, a SPMSM with two pole pairs (p=2) will be considered. Motor parameters and harmonics of the rotor flux density are given in Tables A.1 and A.2 (Appendix A). In practice, the magnitudes of rotor flux density harmonics are determined by an open-circuit test in generator mode. The measured line-to-neutral back force electromotive force (emf) is decomposed in Fourier series, and then the rotor flux density harmonics are calculated according to the method used in [32]. Some of rotor flux density harmonics are attenuated by the distribution of the stator winding and others are cancelled. Therefore, these harmonics will not appear in the back emf. In this study, it is sufficient to take into account the harmonics that produce the emf and are also responsible for torque ripples [32]. The calculation of the torque will be obtained by Equs. (9) and (10), considering the motor running at no load.

3.1 Simulation results in a healthy case

The space harmonics of the stator flux density in healthy case are presented in Fig. 4. In this case it is assumed that the SPMSM is supplied by a by three phase current system. This supply system is a direct balanced one which provides sine currents with I_d=1.7A rms value at 50Hz frequency. In addition to the fundamental, which corresponds to the rank h = p =2, there are space harmonics caused by the non-sine distribution of the winding and by the slots. It can be noticed that the ranks of the harmonics are distributed with respect to h=p(6k+1) (k varies from -∞ to +∞). In Fig.4, these ranks correspond to h=-10 and h=14. This case corresponds to mode 1 in Table 1.

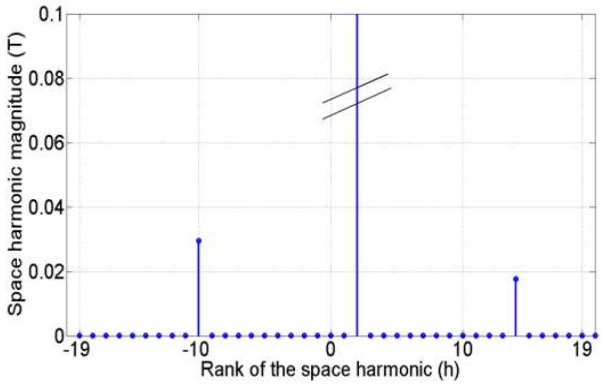

Fig.4. Representation of space harmonic of stator flux density in healthy case

3.2 Simulations results in faulty case

The considered fault model is shown in Fig.5 where a part of the stator winding is short circuited. This approach allows one to consider both stator inter-turn short-circuit fault and lack of turn fault: if $I_{a1} \neq 0, I_f \neq 0$ there is an inter-turn short circuit fault, and if $I_{a1} = 0, I_f \neq 0$ there is a lack of turns fault. Therefore, both faults can be modeled through one model because the torque delivered by the machine depends only on I_{a1}. To simplify

the study, only the lack of turns will be analyzed below, with two different situations: the SPMSM is supplied by balanced and by unbalanced currents

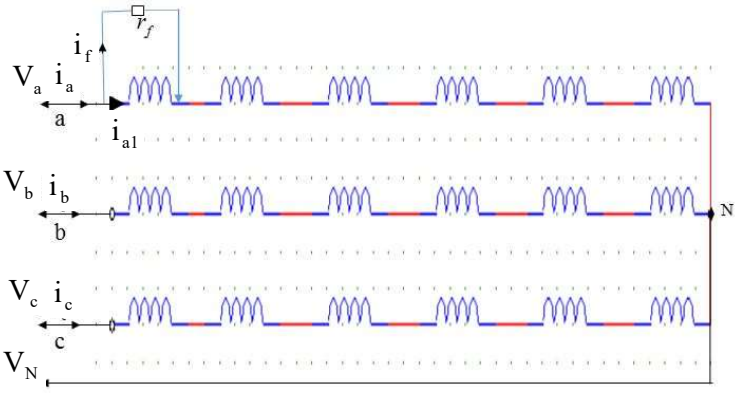

Fig.5. Faulty SPMSM model.

Case 1: balanced current system supplying the faulty SPMSM

For this case, Fig. 6.a shows the space harmonics of the stator flux density where a lack of turns in a stator winding is practically obtained by removing the two thirds of an elementary section in one winding (Fig.10), corresponding to 5.5% of one phase winding. The machine is still supplied by a sine direct balanced three phased current system of magnitude I_d=1.7A rms and 50Hz frequency. It can be noticed that many space flux density harmonics appear, even ones non multiple of p, contrary to a healthy case. The amplitude of stator flux density space harmonic at h=-2 is $B^s_{-2} = 0.023\,\mathrm{T}$.

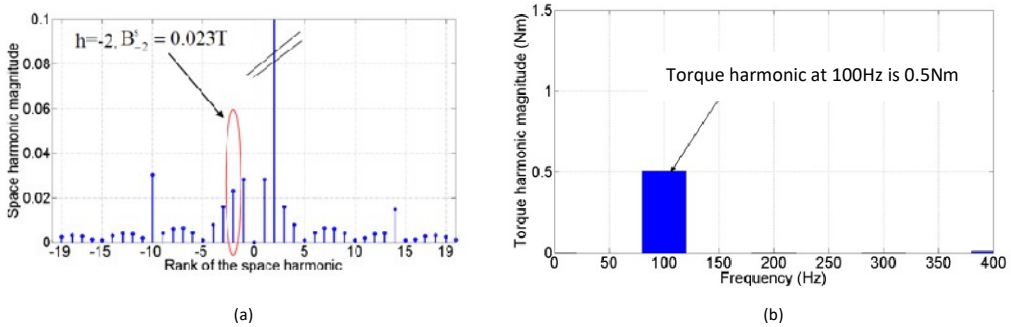

Fig.6. Representation of :(a) space harmonic of stator flux density (b) frequency spectrum of the torque, for the faulty SPMSM supplied by balanced current system.

The torque frequency spectrum in faulty case computed with Equ. (9) and (10) is shown in Fig. 6.b. The harmonic component at 100 Hz corresponding to -h-np = 0 is largely provided by the stator space harmonics flux density at h = -2 and by the rotor space harmonics flux density at n=1. The calculated magnitude of torque harmonic at 100Hz is 0.5Nm. It can be also observed very low magnitude for harmonic at 200Hz, 300Hz, 400Hz generated by combination of rotor harmonic flux density with stator ones. As the amplitudes of flux density harmonics are low, the resulting torque harmonic will have a very low magnitude. The presence of the torque harmonics is baneful for motor because they increase its vibrations and noise [33]. This case corresponds to mode 3 presented in Table 1.

Case 2: unbalanced current system supplying the faulty SPMSM:

Another tested faulty case is presented in Fig. 7, where the faulty SPMSM is supplied by an unbalanced current system. Fig.7.a shows the increase of the amplitude of the flux density space harmonics and Fig.7.b the torque harmonics. In this case, space harmonic of stator flux density at h=-2 is $B^s_{-2} = 0.048\,\mathrm{T}$ and the magnitude of the torque harmonic at 100 Hz is 1.2 Nm, are greater compared to the results presented in Fig.6.b. The unbalanced current system is obtained by supplying the SPMSM with voltage source without current regulation.

In this case, the lack of turns presented in Phase A (Fig. 10) leads to different current values in each phase. These values are reported in mode 2 (Table 1).

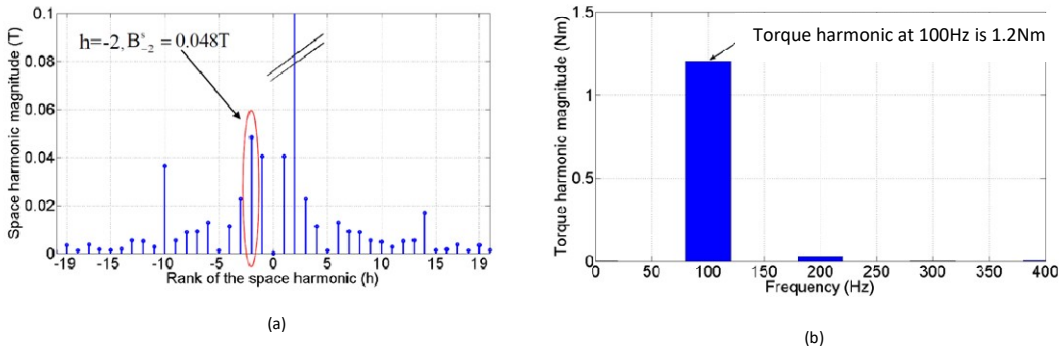

(a) (b)

Fig.7. Representation of: (a) space harmonic of stator flux density, (b) frequency spectrum of the torque for the faulty SPMSM supplied by unbalanced current system.

4 Control procedure for minimizing torque ripples

In order to cancel the torque ripple at 100 Hz frequency, the control is carried out by adding an inverse three phase current system with I_i rms value to the initial direct one. This inverse system will mainly create a space harmonic component of rank h = -2, able to compensate the one generated by the asymmetry.

The strategy for calculation of stator currents able to cancel the space harmonic of the stator flux density at rank h = -2 for a lack of turns fault leads to a relationship between the direct current I_d and the inverse current I_i. The method starts with the knowledge of the currents in the wires in each slot, then the additional inverse system is computed in order to cancel the mmf component at h=-p=-2. The details of the computation leading to the inverse current characteristics are given in Appendix B. Let's assume that the faulty slots are the N°3 and 10, and that 2/3 of the wires in this slot are missing, then Equ. B.7 has to be considered with p=2, K=2/3 and I_{al}=0, leading to:

$$\bar{I}_i = \frac{2}{3} I_d \sum_{j=3,10} e^{j(-2\beta_j^s+\varphi_{dj})} / \sum_{j=1}^{N_t^s} e^{j(-2\beta_j^s+\varphi_{ij})} \qquad (11)$$

The computation gives $I_i = I_d/27$ and for I_d =1.7A rms and I_i=0.064A rms (mode 4 in Table 1). The injection of the inverse current calculated previously allows the reduction of the harmonic at rank h=-2 of stator flux density as shown in Fig.8.a.

In Fig.8.b the torque spectrum after injection of the inverse current is presented. It can be seen that there is a strong decrease of the 100Hz harmonic torque, whereas the other harmonics still have low values.

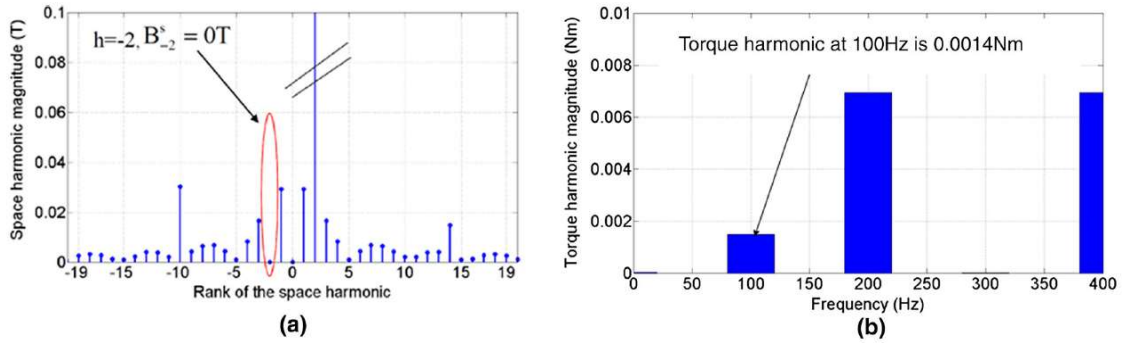

(a) (b)

Fig.8. Representation of: (a) space harmonic of stator flux density (b) frequency spectrum of the torque in faulty case after injection of inverse current.

5 Experimental results

Experiments are performed on a laboratory test bench. A block diagram and a picture of the test bench are presented in Fig. 9. The used SPMSM is the same machine studied in the theoretical analysis with the following electrical characteristics: 4.4 kW rated power, 1500 rpm rated speed, 4-pole. The stator windings are concentric, with 3 elementary sections per pole per phase that can be used to generate faults such as a lack of turns or a short-circuit of a part of an elementary section (Fig.10). The machine is supplied by a power amplifier (Model 390-ASX - Pacific Power Source), controlled by a PC such that magnitudes and phase angles of the voltages can be adjusted. Supply currents can be adjusted indirectly by tuning these variables. The torque is not directly measured but the presence of torque harmonics is evaluated through the tangential vibrations they generate. An accelerometer with 0.01mV/mms^{-2} sensitivity is suitably placed in order to measure the tangential vibrations of the machine. It is connected to a frequency analyzer (Brüel&Kjær 3560).

The aim of the experiments is to test the impact of the new reference current on the reduction of the tangential vibrations at 100 Hz generated by the faulty SPMSM. The considered fault is, according to the theoretical analysis, a lack of turns of 2/3 from the elementary section located in phase A (Fig.10). Voltages, currents, and tangential vibrations are recorded for 4 operating modes of the SPMSM, as presented in the simulation:

- mode 1: *healthy* SPMSM supplied by a balanced voltage and current systems.
- mode 2: *faulty* SPMSM supplied by a balanced voltage and an unbalanced amplitude currents system.
- mode 3: *faulty* SPMSM supplied by balanced currents system
- mode 4: *faulty* SPMSM supplied by unbalanced currents system, minimizing the 100Hz harmonic torque component.

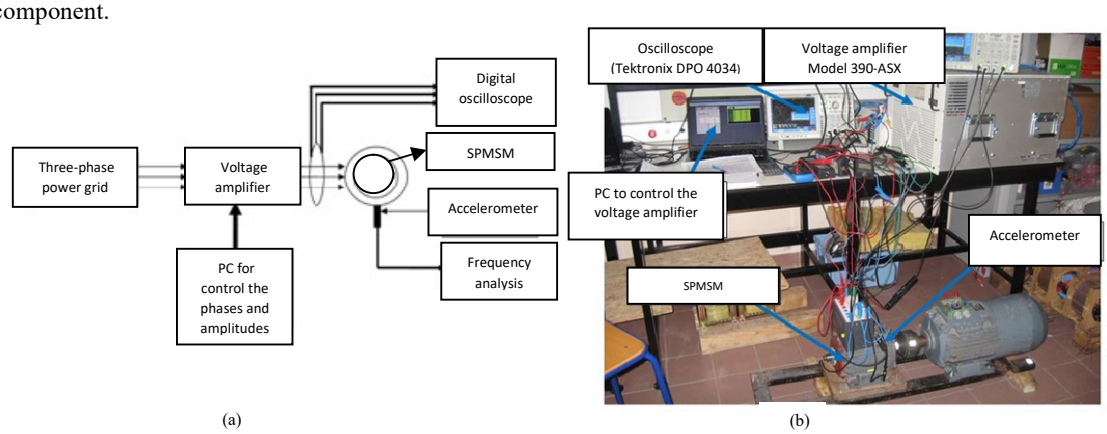

Fig.9. Experimental test bench: (a) block diagram (b) picture of the laboratory test bench.

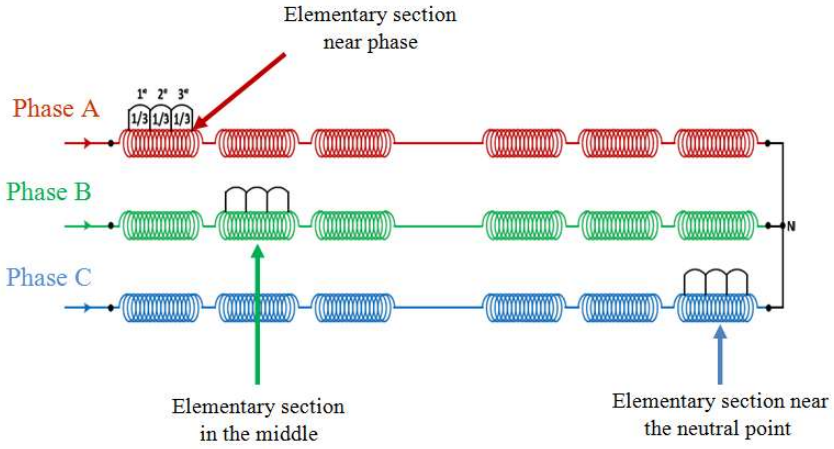

Fig.10. Stator winding

In mode 1, the recorded voltages of each phase (V_a,V_b,V_c) and current (I_a, I_b, I_c) supplying the SPMSM are shown in Fig.11. It can be noticed that the corresponding three phase systems are balanced. All measured values are reported in Table 1. The torque harmonics of the healthy SPMSM are evaluated by measuring the tangential vibrations. The spectrum measured is given in Fig.12. The cursor gives 2.97mV amplitude for the 100Hz

component from the signal delivered by the accelerometer; its amplitude is lower than the magnitude of harmonics at 25Hz and 50Hz.

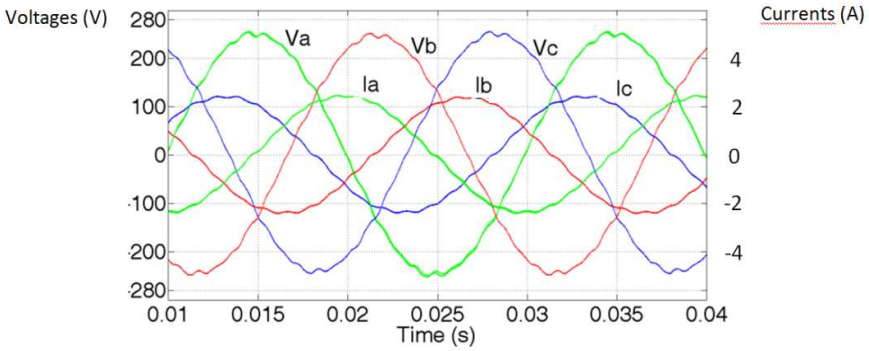

Fig.11. Voltages and currents delivered by balanced system supplying the healthy SPMSM (mode 1).

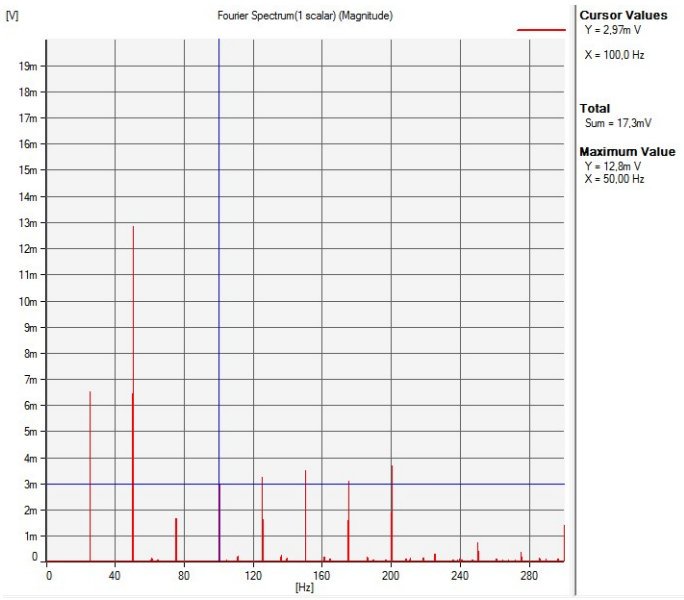

Fig.12. Spectrum of tangential vibrations signal generated by the healthy SPMSM supplied by balanced current system (mode 1), 0.01mV/mms^{-2}.

Demagnetization and eccentricity faults produce vibration at $f = 2\pi(1 \pm k/p)$ $k = 1,2,3....$ as reported in [6], [7] and [9]; this assumption can justify the presence of vibration spectral lines at 25 Hz, 50 Hz, and 75 Hz.

When a fault occurs, three cases are analyzed. The first one considers the faulty SPMSM supplied by a balanced voltage system. This case leads to unbalanced currents in the motor phases (mode 2) as shown in Fig.13. In the winding with lack of turns (in phase A), it can be observed that the amplitude of I_a is greater than the amplitudes of I_b, I_c. In this case, the amplitude of tangential vibrations at 50 Hz and 100 Hz (Fig.14) become respectively 23.8 mV and 8.94 mV, and are greater than the ones relative to the healthy machine shown in Fig.12.

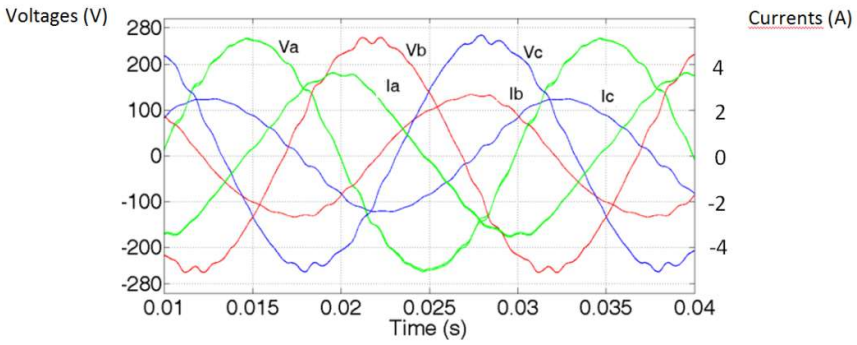

Fig.13. Unbalanced currents delivered by balanced voltage system supplying the faulty SPMSM (mode 2).

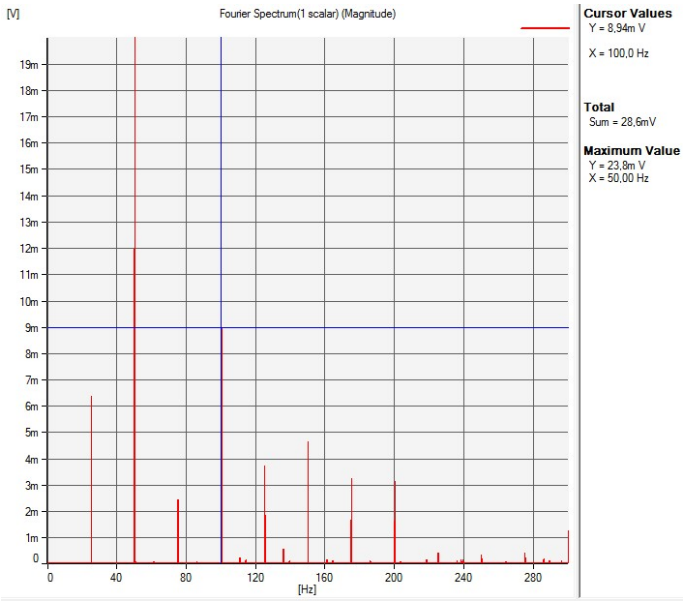

Fig.14. Spectrum of tangential vibrations signal generated by the faulty SPMSM supplied by unbalanced currents system (mode 2) 0.01mV/mms^{-2}.

In the second faulty case, supply voltages are adjusted in order to provide balanced currents in the three phases (mode 3) of the SPMSM (Fig. 15).The results, regarding the tangential vibration spectrum, are presented in Fig.16. It can be seen that the harmonic amplitude at 100Hz is more reduced (3.84 mV) compared to the value relative to mode 2 (Fig.14).

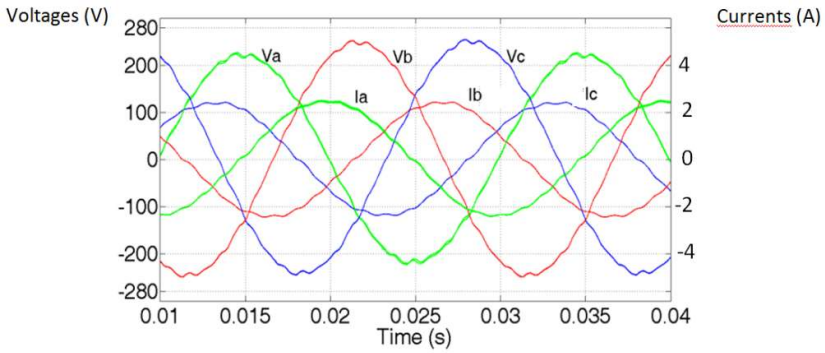

Fig.15. Balanced currents delivered by unbalanced system in voltage amplitude supplying the faulty SPMSM (mode 3).

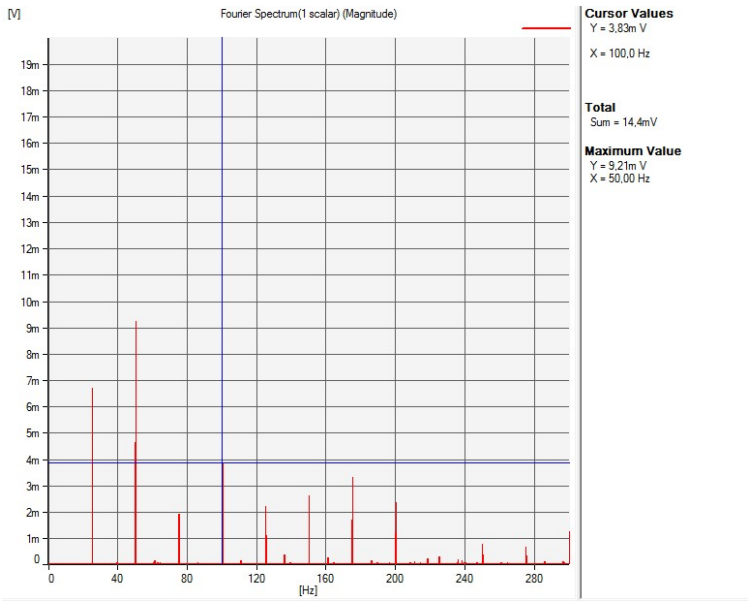

Fig.16. Spectrum of tangential vibrations signal generated by the faulty SPMSM supplied by balanced system in current amplitude(mode 3).

The third analyzed case corresponds to mode 4 (Fig.17) where the phase and the amplitude of the currents are adjusted in order to reduce the tangential vibrations. For that, I_a, I_b and I_c are computed from the inverse current I_i and the direct current I_d using the following transform.

$$\begin{bmatrix} \bar{I}_a \\ \bar{I}_b \\ \bar{I}_c \end{bmatrix} = \begin{bmatrix} 1 & 1 & 1 \\ a^2 & a & 1 \\ a & a^2 & 1 \end{bmatrix} \cdot \begin{bmatrix} \bar{I}_d \\ \bar{I}_i \\ 0 \end{bmatrix} \qquad (12)$$

where $a = \exp(i\frac{2\pi}{3})$, $\bar{I}_a = I_a \exp(i\varphi_a), \bar{I}_b = I_b \exp(i\varphi_b), \bar{I}_c = I_c \exp(i\varphi_c)$, i is the complex number such that $i^2=-1$.

Actually, I_d is imposed and the phase and amplitude of I_i are adjusted in order to minimize the 100Hz tangential vibration harmonic. The frequency spectrum of tangential vibrations measured by the accelerometer is presented in Fig.18. The currents become unbalanced and it can be seen that the amplitude of the harmonic at 100Hz is more reduced (3.19 mV) than the amplitude relative to the mode 2 (Fig.14 - 8.94mV) and the value obtained in the mode 3 (Fig.16 - 3.84mV). Computed and measured values of the currents (amplitude, phase), the 100Hz harmonics torque component and the 100Hz tangential vibration are reported in Table 1.

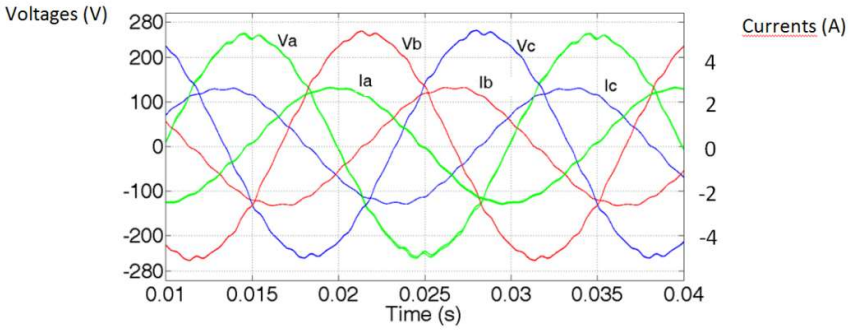

Fig.17. Voltages and currents delivered by unbalanced system in voltage amplitude and phase supplying the faulty SPMSM (mode 4).

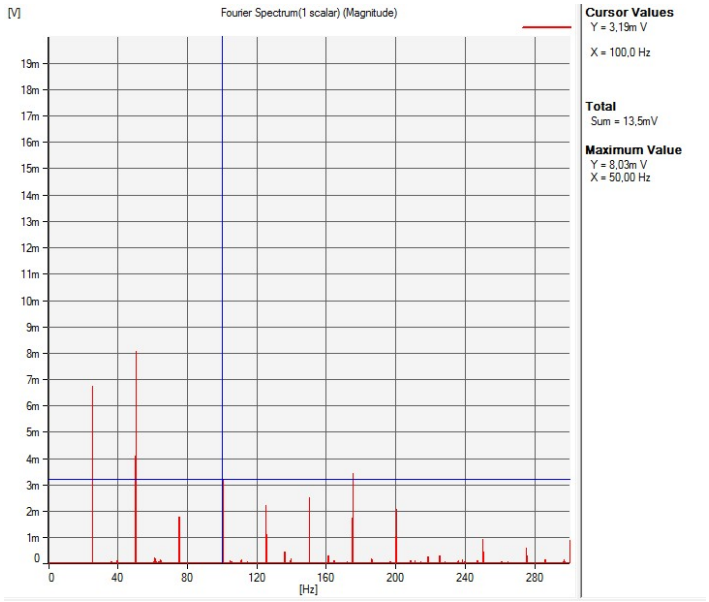

Fig.18. Spectrum of tangential vibrations signal generated by the faulty SPMSM supplied by unbalanced system in voltage amplitude and phase (mode 4).

In order to compute the direct and inverse current from measurements, Equ. (13) and Equ. (14) are used :

$$\bar{I}_d = \frac{1}{3}(\bar{I}_a + a\bar{I}_b + a^2\bar{I}_c) \tag{13}$$

$$\bar{I}_i = \frac{1}{3}(\bar{I}_a + a^2\bar{I}_b + a\bar{I}_c) \tag{14}$$

It can be noticed a good concordance between simulations $\left|\frac{I_d}{I_i}\right| \approx 26$ and experimental $\left|\frac{I_d}{I_i}\right| \approx 21$ results in mode 4 when an inverse current is injected to decrease the amplitude of harmonic at 100 Hz. This case is denoted by “inj” parameter in Table 1.

6 Conclusion

In this paper, a method for analyzing the stator flux density in faulty conditions has been presented. The role of the space harmonics in torque harmonics generation is brought to the fore. As far as stator winding asymmetry is considered, a method for reducing the torque harmonic at 100 Hz frequency, based on the reduction of the stator flux density harmonic of rank h= -2, has been studied analytically. Actually, the torque harmonic at 100 Hz is generated by an inverse current system or by a stator winding asymmetry. Each one creates a significant harmonic flux density of rank h = -p, and the approach presented in this paper aims at using the inverse stator current to compensate the flux density harmonic h = -p generated by the winding asymmetry. The case of stator lack of turns is illustrated in the paper as stator asymmetry but actually the computation can also be applied in the case of a stator inter-turns short circuit. The experimental results confirm the analytical study and shows that the tangential vibrations caused by torque ripples can be reduced by unbalancing the current system supplying the faulty SPMSM.

Table 1. Summary table with experimental and simulation results for healthy and faulty case of the SPMSM supplied by balanced (b) and unbalanced (u) currents. Vibration variation obtained by injection of inverse current (inj).

	Experimental results				Simulation results			
Case	Healthy	Faulty			Healthy	Faulty		
		u	b	inj		u	b	inj
Mode	1	2	3	4	1	2	3	4
Torque harmonic at 100 Hz [Nm]					0	1.2	0.5	0.0014
Amplitude of vibration harmonic at 50 Hz [mv]	12.8	23.8	9.21	8.03				
Amplitude of vibration harmonic at 100 Hz [mv]	2.97	8.94	3.83	**3.19**				
I_a [A]	1.69	2.43	1.70	1.86	1.7	2.43	1.7	1.76
I_b [A]	1.70	1.73	1.70	1.84	1.7	1.73	1.7	1.66
I_c [A]	1.71	1.89	1.70	1.84	1.7	1.893	1.7	1.66
φ_a Phase A	0°	0°	0°	0°	0°	0°	0°	0°
φ_bPhase B	240°	240°	241.21°	248.66°	240°	240°	240°	239°
φ_c Phase C	120°	120°	122.2°	120.89°	120°	120°	120°	121°
I_d	1.70 + 0.0044i	1.9460 + 0.0044i	1.6994 + 0.0340i	1.8395 + 0.1019i	1.7	1.9460 + 0.0044i	1.7	1.7
I_i	0.0038 - 0.0022i	0.2498 - 0.0022i	0.0126 - 0.0166i	-0.0732 - 0.0513i	0	0.2498 - 0.0022i	0	0.0630
$\left\|\frac{I_d}{I_i}\right\|$	390.65	7.50	81.37	**20.61**		7.50		**26.57**

APPENDIX A

Table.A.1. SPMSM parameter simulation

Rotor flux density space harmonic magnitudes (Tesla)							
B_1^r	B_3^r	B_5^r	B_7^r	B_9^r	B_{11}^r	B_{13}^r	B_{15}^r
0.5711	0.0080	0.0966	0.0668	0.0030	0.0350	0.0308	0.0026

Table.A.2. Rotor flux density space harmonic

SPMSM parameters								
p	n_e	N_t^s	Ω (rad/s)	K	l_e^s (cm)	l_d^s(cm)	p^s	e(mm)
2	36	36	157	1/3	0.27	0.7368	$l_e^s/5$	0.5

APPENDIX B

The strategy for calculation of stator currents consists in cancelling the space harmonic of stator mmf of rank h = -p in the case of a stator fault in one phase winding. The computation of a mmf space harmonic component is done by considering the currents in each slot. The following developments consider p pole pair machine with an inter-turn short circuit fault that occurs in slots j_1 and j_2. K is the ratio of faulty windings in the faulty slots, I_{a1} is the rms value of the current in the faulty turns.

Let us consider the mmf ε_j^s generated by the n^e wire placed in slot j. The wave form of ε_j^s is shown in Fig. B.1

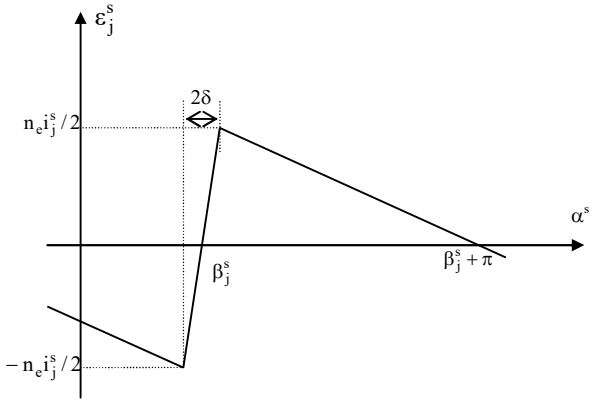

Fig. B.1 – mmf generated by the wires in one slot

ε_j^s can be written with a Fourier series as follows:

$$\varepsilon_j^s = \frac{n_e i_j^s}{(\pi-\delta)} \sum_{h=1}^{+\infty} \Gamma_h \frac{\sin\left(h(\alpha^s - \beta_j^s)\right)}{h} = \sum_{h=1}^{+\infty} \varepsilon_{j,h}^s$$

The analytical computation is performed using the complex notation of the mmf components when the SPMSM is assumed to be supplied with sine currents: $i_j^s = \sqrt{2}\, I_j^s \sin(\omega t + \varphi_j)$

Then, the complex quantity $\underline{\varepsilon}_{j,h}^s$ is defined such that

$$\varepsilon_{j,h}^s = \Re\left[\underline{\varepsilon}_{j,h}^s e^{i(\omega t - h\alpha^s)}\right]$$

And the rank h of mmf harmonic generated by all the slots can be expressed as :

$$\varepsilon_h^s = \sum_{j=1}^{N_s^t} \varepsilon_{j,h}^s = \Re\left[e^{i(\omega t - h\alpha^s)} \sum_{j=1}^{N_t^s} \underline{\varepsilon}_{j,h}^s \right]$$

Case of inter-turn short circuit fault in stator winding:

The stator winding mmf at h=-p is computed in two cases:

- healthy stator winding supplied by direct current of I_d rms value, in this case the mmf harmonic at h=-p is null, because in healthy case only the ranks h=p(6k+1) exist.

$$\underline{\varepsilon}_{d-p}^s = \sum_{j=1}^{N_t^s} \frac{n_j^e I_d}{\sqrt{2}\,(\pi - \delta)(-p)} \Gamma_{-p} e^{i(-p\,\beta_j^s + \varphi_{dj})} = 0 \qquad \text{(B.1)}$$

- faulty stator winding supplied by direct current of I_d rms value. In this case Kn^e wires of the slots j_1 an j_2 are flowed through by a current of I_{a1} magnitude and the other wires of the both slots ((1-K)n^e wires) are flowed through by the line current of I_d magnitude. :

$$\bar{\varepsilon}^{s}_{d,-p(fault)} = \sum_{\substack{j=1 \\ j\neq j_1,j_2}}^{N_t^s} \frac{n^e I_d}{\sqrt{2}(\pi-\delta)(-p)}\Gamma_{-p} e^{i(-p\beta_j^s+\varphi_{dj})} + \sum_{j=j_1,j_2} \frac{Kn^e I_{a1}}{\sqrt{2}(\pi-\delta)(-p)}\Gamma_{-p} e^{i(-p\beta_j^s+\varphi_{a1dj})} + \sum_{j=j_1,j_2} \frac{(1-K)n^e I_d}{\sqrt{2}(\pi-\delta)(-p)}\Gamma_{-p} e^{i(-p\beta_j^s+\varphi_{dj})} \quad (B.2)$$

For the stator winding supplied by inverse current of I_i rms value, it is supposed that the inverse current does not flow through the fault resistance r_f, the stator winding mmf at h=-p can be expressed as follows:

$$\bar{\varepsilon}^{s}_{i,-p\ (fault)} = \sum_{j=1}^{N_t^s} \frac{n^e \bar{I}_i}{\sqrt{2}(\pi-\delta)(-p)}\Gamma_{-p} e^{i(-p\ \beta_j^s+\varphi_{ij})} \quad (B.3)$$

To cancel the harmonic h = -p, the mmf generated by the inverse and direct current must satisfy the following equation:

$$\bar{\varepsilon}^{s}_{i,-p(fault)} = \bar{\varepsilon}^{s}_{d,-p} - \bar{\varepsilon}^{s}_{d,-p(fault)} \quad (B.4)$$

Then it comes:

$$\bar{\varepsilon}^{s}_{i,-p(fault)} = \sum_{j=j_1,j_2} \frac{n^e}{\sqrt{2}(\pi-\delta)(-p)}\Gamma_{-p}\left(I_d e^{i(-p\beta_j^s+\varphi_{dj})} - KI_{a1} e^{i(-p\beta_j^s+\varphi_{a1dj})} - (1-K)I_d e^{i(-p\beta_j^s+\varphi_{dj})}\right)$$

Replacing $\varepsilon^{s}_{i,-p(fault)}$ with (B.3), it comes:

$$\sum_{j=1}^{N_t^s} \frac{n^e \bar{I}_i}{\sqrt{2}(\pi-\delta)(-p)}\Gamma_{-p} e^{i(-p\beta_j^s+\varphi_{ij})} = \sum_{j=j_1,j_2} \frac{n^e}{\sqrt{2}(\pi-\delta)(-p)}\Gamma_{-2}\left(I_d e^{i(-p\beta_j^s+\varphi_{dj})} - KI_{a1} e^{i(-p\beta_j^s+\varphi_{a1dj})} - (1-K)I_d e^{i(-p\beta_j^s+\varphi_{dj})}\right) \quad (B.5)$$

Finally, after simplification, the relationship between the direct current and the inverse current used to compensate the harmonic of rank h=-p is given by:

$$\bar{I}_i = \frac{\sum_{j=j_1,j_2}\left(I_d e^{i(-p\beta_j^s+\varphi_{dj})} - KI_{a1} e^{i(-p\beta_j^s+\varphi_{a1dj})} - (1-K)I_d e^{i(-p\beta_j^s+\varphi_{dj})}\right)}{\sum_{j=1}^{N_t^s} e^{i(-p\beta_j^s+\varphi_{ij})}} \quad (B.6)$$

And finally:

$$\bar{I}_i = K\frac{I_d \sum_{j=j_1,j_2} e^{i(-p\beta_j^s+\varphi_{dj})} - I_{a1} \sum_{j=j_1,j_2} e^{i(-p\beta_j^s+\varphi_{a1dj})}}{\sum_{j=1}^{N_t^s} e^{i(-p\beta_j^s+\varphi_{ij})}} \quad (B.7)$$

References

[1] Li S, Xia C, Zhou X (2012) Disturbance rejection control method for permanent magnet synchronous motor speed-regulation system. Mechatronics 22: 706–714

[2] Borghi C A, Casadei D, Fabbri M, Serra G (1998). Reduction of the torque ripple in permanent magnet actuators by a multi-objective minimization technique. IEEE Trans. Magnetics 34: 2869- 2872

[3] Mohamed Y A-R I, Newly A (2007). Designed instantaneous-torque Ccntrol of direct-drive PMSM servo actuator with improved torque estimation and control characteristics. IEEE Trans. Ind. Electron. 54: 2864 - 2873

[4] Pellegrino G, Guglielmi P, Vagati A, Villata F (2010). Core losses and torque ripple in IPM machines: dedicated modeling and design tradeoff. IEEE. Trans.Ind. Applicat. 46: 2381-2391

[5] Mademlis C, Margaris N (2002). Loss minimization in vector-controlled interior permanent-magnet synchronous motor drives. IEEE Trans. Ind.Electron. 49: 1344-1347

[6] Ebrahimi B M, Faiz J (2012). Configuration impact on eccentricity fault detection in permanent magnet synchronous motors. IEEE Trans. Magnetics 48: 903-906

[7] Ebrahimi B M, Roshtkhari M J, Faiz J, Khatami S V (2014). Advanced eccentricity fault recognition in permanent magnet synchronous motors using stator current signature analysis. IEEE Trans. Ind.Electron. 61: 2041-2052

[8] Byong I J, Hyon J, Nam K (2013) Dynamic modeling and control for SPMSMs with internal turn short fault. IEEE Trans. Power electron. 28: 3495- 3508

[9] UrrestyJ C, Atashkhooei R, Riba J R, Romeral L, Royo S (2013). Shaft trajectory analysis in a partially demagnetized permanent-magnet synchronous motor. IEEE Trans. Ind.Electron. 60:3454-3461

[10] Brudny J F, Lecointe J P (2011). Rotor design for reducing the switching magnetic noise of ac electrical machine variable-speed drives. IEEE Trans. Ind.Electron. 58: 5112-5120

[11] Leboeuf N, Boileau T, Nahid-Mabarakeh B, Takorabet N, Meibody-Tabar F, Clerc G (2012). Inductance calculations in permanent-magnet motors under fault conditions. IEEE Trans. Magnetics 48: 2605-2616

[12] Romeral L, Urresty J C, Ruiz J R, Espinosa AG (2011). Modeling of surface-mounted permanent magnet synchronous motors with stator winding interturn faults. IEEE Trans. Ind. Electron. 58: 1576-1585

[13] Xu J X, Panda S K, Pan Y J, Lee T H, Lam B H (2004). A modular control scheme for pmsm speed control with pulsating torque minimization. IEEE Trans. Ind. Electron. 51: 526-536

[14] Ait-Gougam Y, Ibtiouen R, Touhami O, Louis J-P, Gabsi M (2008). Inverse modeling and pulsating torque minimization of salient pole non-sinusoidal synchronous machines.Electric Power Systems Research 78: 88–96

[15] Hasanien H.M (2010). Torque ripple minimization of permanent magnet synchronous motor using digital observer controller. Energy Convers and Manage. 51: 98–104

[16] N'diayeA.;EspanetC., MiraouiA.(2004). Reduction of the torque ripples in brushless PM motors by optimization of the supply - theoretical method and experimental implementation. IEEE. Int. Symp.on Industrial Electronics, Ajaccio, France 2-4 May, 2: 1345 – 1350.

[17] Hung JY, Ding Z. (1993). Design of currents to reduce torque ripple in brushless permanent magnet motors.IEE Proceedings B - Electric Power Applications, Vol. 140, N° 4: 260 - 266.

[18] Favre E, Cardoletti L, Jufer M (1993). Permanent-magnet synchronous motors: a comprehensive approach to cogging torque suppression. IEEE. Trans. Ind. Appl. 29: 1141–1149

[19] Jia H, Cheng M, Hua W, Zhao W, Li W (2010). Torque ripple suppression in flux-switching pm motor by harmonic current injection based on voltage space-vector modulation. IEEE Trans. Magnetics 46: 1527-1530

[20] Lee G H, Kim S I, Hong J P, Bahn J H (2008). Torque ripple reduction of interior permanent magnet synchronous motor using harmonic injected current. IEEE Trans. Magnetics 44:1582-1585

[21] Holtz J, Springob L (1996). Identification and compensation of torque ripple in high-precision permanent magnet motor drives. IEEE Trans. Ind. Electron. 43:309–320

[22] Kestelyn X, Semail E (2011). A Vectorial Approach for generation of optimal current references for multiphase permanent-magnet synchronous machines in real time. IEEE Trans. Ind. Electron. 58: 5057-5065

[23] Bennett J W, Jack A G, Mecrow B C, Atkinson D J, Sewell C, Mason G (2004). Fault-tolerant control architecture for an electrical actuator. 35rh Annual IEEE Power Electronics Specialists Conference, Aachen, Gemany 20-25 June: 4371- 4371

[24] Cintron-Rivera JG, Foste SN, Strangas EG (2015). Mitigation of Turn-to-Turn Faults in Fault Tolerant Permanent Magnet Synchronous Motors. IEEE Transactions on Energy Conversion, Vol 30, N°2 : 465 – 475.

[25] Toda H, Xia Z, Wang J, Atallah K, Howe D (2004). Rotor Eddy current loss in permanent magnet brushless machines. IEEE Trans on Magnetics 40:2104-2106

[26] Dajaku G, Gerling D (2012). Air-gap flux density characteristics of salient pole synchronous permanent-magnet machines. IEEE Trans. on Magnetics 48: 2196- 2204

[27] Bianchi N, Fornasiero E (2009). Impact of MMF space harmonic on rotor losses in fractional-slot permanent-magnet machines. IEEE Trans. on Energy Conversion 24:323-328

[28] Ko H S, Kim K J (2004) Characterization of noise and vibration sources in interior permanent-magnet brushless DC motors. IEEE Trans. on Magnetics 40:3482- 3489

[29] Gaussens B, Hoang E, O.de la Barrière, Saint-Michel J, Manfe P, Lécrivain M, Gabsi M (2013). Analytical armature reaction field prediction in field-excited flux-switching machines using an exact relative permeance function. IEEE Trans. on Magnetics 49:628-641

[30] Zhu Z Q, Howe D (1992). Analytical prediction of the cogging torque in radial-field permanent magnet brushless motors. IEEE Trans. on Magnetics 28:1371- 1374

[31] Proca A B, Keyhani A, EL-Antably A, Dai W L M (2003). Analytical model for permanent magnet motors with surface mounted magnets. IEEE Trans. on Energy Conversion 18:386-391

[32] Simon-Sempere V, Burgos-Payan M, Cerquides-Bueno J-R (2012). Spatial filtering: a tool for selective harmonics elimination in the design of permanent –magnet synchronous motors. IEEE Trans. on Magnetics 48: 2056-2067

[33] Sun T, Kim J M, Lee G H, Hong J P, Choi M R (2011). Effect of pole and slot combination on noise and vibration in permanent magnet synchronous motor. IEEE Trans. on Magnetics 47: 1038-1041